

Passively Safe Receding Horizon Control for Satellite Proximity Operations

Marcus Holzinger, Jeremiah DiMatteo, Jeremy Schwartz, and Mark Milam

Abstract—Recent on-orbit mission performance illustrates a pressing need to develop passively safe formation flight trajectories and controllers for multiple satellite proximity operations. A Receding Horizon Control (RHC) approach is formulated that directly relates navigation uncertainty and process noise to non-convex quadratic constraints, which enforce passive safety in the presence of a large class of navigation or propulsion system failures. Several Keplerian simulations are executed to examine increased Δv usage incurred by adding passive safety constraints, the corresponding reduction in collision probability, and resulting passively safe formation flight geometries. Results show that modest cross-track motion significantly reduces collision probability, and that once a passively safe relative orbit is achieved, steady-state Δv usage rates are comparable to usage rates without passive safety constraints. Navigation uncertainty and process noise are found to be significant Δv usage drivers for passively safe proximity operations. On-orbit autonomous RHC control with passive safety constraints applied to proximity operation missions enables trajectory generation and control that reduces collision probability to acceptable levels while minimizing Δv usage.

I. INTRODUCTION

Satellite collision avoidance is a paramount concern in proximity operations. In April, 2005 the Demonstration for Autonomous Rendezvous Technology (DART) satellite collided with its rendezvous target MUBLCOM [1]. Satellite proximity operations, specifically collision avoidance in the event of catastrophic failure, is vulnerable to relative navigation filter inaccuracy or disruption. Passive safety (PS), previously defined as relative trajectories that “guarantee collision avoidance with no thrusting required ... in the presence of a class of anomalous system behaviors” [2], is a potential solution to the type of anomalous system behavior experienced by DART.

Baseline operational mission requirements for PS during proximity operations can be summarized as:

- 1) The individual satellites shall maintain a relative distance of less than X km between any two satellites.
- 2) The individual satellites shall maintain passive safety with respect to all other satellites, active or inactive, within Y km, with a maximum collision probability of 10^{-6} over a failure duration of Z orbits. Failures include complete loss of navigation capability or control authority.

Navigation uncertainty is central to the discussion of passive safety. Several studies suggest that many traditional relative states/maneuvers in proximity operations are not passively safe [3,4,5]. Particularly, [5] shows that relative

state knowledge uncertainty in the satellite’s along-track direction grows significantly faster than either the radial or cross-track, and emphasizes that relative velocity uncertainty dominates uncertainty propagation. Accordingly, stationary satellites on the along-track axis or on a small relative motion ellipse exclusively in the orbit plane potentially have a high probability of collision.

Previous work [2] addresses the concern for potential satellite collision resulting from navigation uncertainty. Applying techniques used in [6,7] passively safe relative trajectories may be generated that guarantee safety for a specific initial state or finite set of initial states. Classes of failures considered include loss of navigation capability and loss of control authority. Process noise is separately addressed by determining the expected worst case disturbance inputs and designing an optimal trajectory that is robust against them.

Past efforts also show the utility and feasibility of employing Linear Programming (LP) and Mixed-Integer Linear Programming (MILP) methods to proximity operations, both in trajectory generation and Model Predictive Control (MPC) or, equivalently, Receding Horizon Control (RHC) settings [2,6,7]. Control input, control input rate, periodic, and relative position/velocity constraints are used. However, existing proximity operations RHC implementations do not account for initial state uncertainty and process noise in an explicit stochastic sense, and do not guarantee a specific collision probability for a fixed period of time.

Using a-priori or real-time navigation uncertainty knowledge, this paper formulates constraints that enforce passive safety with a known probability for a fixed period of time in the event of navigation or propulsion system failure. The relative navigation control implementation is formulated as a RHC problem and stability is examined for circular orbits. The closed-loop RHC is applied to Keplerian proximity operations simulations to demonstrate both utility and robustness. The increased Δv usage incurred by adding passive safety constraints is examined, the corresponding reduction in collision probability is quantified, and resulting passively safe relative orbit geometries are observed. Relative navigation uncertainty is varied and its effects on relative orbit geometry changes and Δv to maintain passive safety is analyzed. Additional proximity costs to further constrain relative motion while maintaining passive safety are developed and performance metrics are examined.

II. PROBLEM FORMULATION

Previous work on satellite proximity operations formulate the trajectory planning problem as an LP optimization using

Lawden's [8] relative dynamic equations, which are useful for applications on eccentric reference orbits [2,6,7]. The problem formulation is kept in terms of a generic set of Linear, Time-Varying (LTV) or Linear Parameter-Varying (LPV) differential equations. The discrete-time equations for the following formulation are written as

$$\mathbf{x}_{k+1} = \Phi_{k,k+1}\mathbf{x}_k + \Gamma_{k,k+1}\mathbf{u}_k, \quad (1)$$

with the implicit understanding that the equations can represent either the LTV or LPV dynamics (and as a special case, Hill's or Clohessy-Wiltshire (CW) equations [9, 10]).

A. Passive Safety Constraint

Relative state uncertainty between satellites, such as the Chaser and Resident Space Objects (RSOs) shown in figure 1, must be considered when formulating passive safety constraints. For a given system, the covariance matrix \mathbf{P} represents the navigation uncertainty error ellipsoid (of size $1-\sigma$). Given a relative navigation error covariance matrix \mathbf{P}_k at time k , uncertainty propagation is described by [11] as

$$\mathbf{P}_{k+1} = \Phi_{k,k+1}\mathbf{P}_k\Phi_{k,k+1}^T + \Gamma_{k,k+1}\mathbf{Q}_k\Gamma_{k,k+1}^T. \quad (2)$$

If the covariance matrix \mathbf{P}_{k+1} is generated by a Kalman filter, the navigation uncertainty ellipsoid at time $k+1$ incorporates evolving navigation uncertainty and process noise at time k . The passive safety constraint is enforced by ensuring that the RSOs are guaranteed with $\alpha-\sigma$ certainty to be outside the uncertainty ellipsoid of size $\alpha-\sigma$ centered about the Chaser at time step k . Figure 1 depicts the passive safety constraint with the $\alpha-\sigma$ uncertainty ellipsoid centered about the Chaser. The Chaser and RSOs are assumed to be drifting for f time steps according to relative motion dynamics.

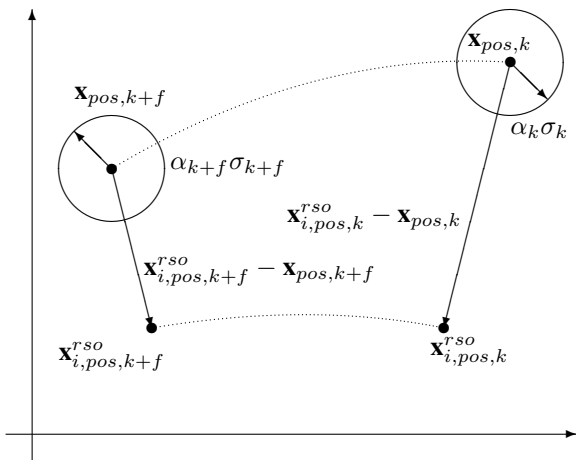


Fig. 1. Relative position and position uncertainty of the RSO $\mathbf{x}_{i,pos}^{rso}$ and Chaser \mathbf{x}_{pos} at time step k and $k+f$

Requiring the relative position between the i^{th} RSO \mathbf{x}_i^{rso} and the Chaser \mathbf{x} to be outside an uncertainty ellipse of size

$\alpha-\sigma$ centered at the Chaser at time k yields the following constraint:

$$\frac{(x_{i,r,k}^{rso} - r_k)^2}{\alpha_k^2 \sigma_{r,k}^2} + \frac{(x_{i,s,k}^{rso} - s_k)^2}{\alpha_k^2 \sigma_{s,k}^2} + \frac{(x_{i,w,k}^{rso} - w_k)^2}{\alpha_k^2 \sigma_{w,k}^2} \geq 1,$$

where

$$\mathbf{x}_{i,pos,k}^{rso} = \begin{bmatrix} x_{i,r,k}^{rso} & x_{i,s,k}^{rso} & x_{i,w,k}^{rso} \end{bmatrix}$$

and

$$\mathbf{x}_{pos,k} = \begin{bmatrix} r_k & s_k & w_k \end{bmatrix}.$$

This constraint is more conveniently expressed as

$$\begin{aligned} \left[\mathbf{x}_{i,pos,k}^{rso} - \mathbf{x}_{pos,k} \right]^T \mathbf{P}_{pos,k}^{-1} \left[\mathbf{x}_{i,pos,k}^{rso} - \mathbf{x}_{pos,k} \right] &\geq \alpha_k^2 \\ \left[\mathbf{x}_{i,k}^{rso} - \mathbf{x}_k \right]^T \tilde{\mathbf{P}}_k \left[\mathbf{x}_{i,k}^{rso} - \mathbf{x}_k \right] &\geq \alpha_k^2, \end{aligned}$$

where $\mathbf{P}_{pos,k}$ is the 3×3 position covariance matrix, and

$$\tilde{\mathbf{P}}_k = \begin{bmatrix} \mathbf{I}_{3 \times 3} \\ \mathbf{0}_{3 \times 3} \end{bmatrix} \mathbf{P}_{pos,k}^{-1} \begin{bmatrix} \mathbf{I}_{3 \times 3} & \mathbf{0}_{3 \times 3} \end{bmatrix}$$

A similar ellipsoid representation is also proposed for safety purposes in [5]. In the event of a navigation or control failure, the system drifts and is propagated f time steps using (1) with the control inputs \mathbf{u} set to zero:

$$\begin{aligned} \mathbf{x}_{k+f} &= [\Phi_{k+f-1,k+f} \cdots \Phi_{k+1,k+2} \Phi_{k,k+1}] \mathbf{x}_k \\ \mathbf{x}_{k+f} &= \tilde{\Phi}_{k,k+f} \mathbf{x}_k \end{aligned}$$

Similarly, the relative state $\mathbf{x}_{i,k}^{rso} - \mathbf{x}_k$ may be propagated forward in time as

$$\left[\mathbf{x}_{i,k+f}^{rso} - \mathbf{x}_{k+f} \right] = \tilde{\Phi}_{k,k+f} \left[\mathbf{x}_{i,k}^{rso} - \mathbf{x}_k \right].$$

This allows the ellipsoid constraint at time k to be expressed as

$$\left[\mathbf{x}_{i,k}^{rso} - \mathbf{x}_k \right]^T \tilde{\Phi}_{k,k+f}^T \tilde{\mathbf{P}}_{k+f} \tilde{\Phi}_{k,k+f} \left[\mathbf{x}_{i,k}^{rso} - \mathbf{x}_k \right] \geq \alpha_{k+f}^2, \quad (3)$$

where the relative states and uncertainty may be propagated f steps. Constraint formulation (3) is non-convex, has a non-empty null-space, and ensures passive safety at time $k+f$. To ensure that the Chaser state is passively safe if the Chaser were to start drifting at time k for an additional f steps, multiple constraints of the type shown in (3) must be introduced. For each step k in the optimization problem, the entire drift trajectory of f steps must also be passively safe. This is enforced by

$$\begin{bmatrix} \left[\mathbf{x}_{i,k}^{rso} - \mathbf{x}_k \right]^T \tilde{\mathbf{P}}_k \left[\mathbf{x}_{i,k}^{rso} - \mathbf{x}_k \right] \\ \left[\mathbf{x}_{i,k}^{rso} - \mathbf{x}_k \right]^T \tilde{\Phi}_{k,k+1}^T \tilde{\mathbf{P}}_{k+1} \tilde{\Phi}_{k,k+1} \left[\mathbf{x}_{i,k}^{rso} - \mathbf{x}_k \right] \\ \vdots \\ \left[\mathbf{x}_{i,k}^{rso} - \mathbf{x}_k \right]^T \tilde{\Phi}_{k,k+f}^T \tilde{\mathbf{P}}_{k+f} \tilde{\Phi}_{k,k+f} \left[\mathbf{x}_{i,k}^{rso} - \mathbf{x}_k \right] \end{bmatrix} \geq \bar{\alpha} \quad (4)$$

where $\bar{\alpha} = \left[\alpha_k^2, \alpha_{k+1}^2, \dots, \alpha_{k+f}^2 \right]^T$. The size and number of drift constraints f for time step k must be chosen to ensure that passive safety is not violated between discretization points. Enforcing passive safety as shown above adds $f+1$

non-convex quadratic constraints for each RSO \mathbf{x}_i^{rso} . The advantage of explicitly using \mathbf{P} to ensure passive safety is clear; the relative navigation uncertainty and process noise are accounted for, and the propagated uncertainty ellipsoid constraints are satisfied.

1) *Quantifying Collision Probability*: An analytical probability of collision metric P_{col} that accounts for satellite dimensions and navigation uncertainty is calculated to measure the effectiveness of the passive safety constraint (4). Defining the relative position error between the Chaser and a i^{th} RSO as $\mathbf{e}_k = \mathbf{x}_{i,pos,k}^{rso} - \mathbf{x}_{pos,k}$, the probability density function $PDF(\mathbf{e}(k))$ described by [12] for multivariate Gaussian distributions is written as

$$PDF(\mathbf{e}_k) = \left[(2\pi)^{\frac{3}{2}} |\mathbf{P}_{pos,k}|^{\frac{1}{2}} \right]^{-1} e^{-\frac{1}{2} \mathbf{e}_k^T \mathbf{P}_{pos,k}^{-1} \mathbf{e}_k},$$

with $\mathbf{x}_{pos,k}$, $\mathbf{x}_{i,pos,k}^{rso}$, and $\mathbf{P}_{pos,k}$ having the same definitions as the last section, and $|\cdot|$ is defined as the matrix determinant operator. The instantaneous probability of collision between the Chaser and a RSO is defined as

$$P_{col,\mathbf{V}}(\mathbf{e}_k) = \int_{\mathbf{V}} \left[(2\pi)^{\frac{3}{2}} |\mathbf{P}_{pos,k}|^{\frac{1}{2}} \right]^{-1} e^{-\frac{1}{2} \mathbf{e}_k^T \mathbf{P}_{pos,k}^{-1} \mathbf{e}_k} d\mathbf{V}, \quad (5)$$

where the volume integral limits are defined by the volume \mathbf{V} about the Chaser position $\mathbf{x}_{pos,k}$. The uncertainty ellipsoid size α_k directly affects the collision probability and is selected via trial and error to ensure that the calculated $P_{col,\mathbf{V}}(\mathbf{e}_k)$ is less than 10^{-6} .

B. Relative Proximity Constraint

Relative proximity is enforced by requiring that a set of propagated states be within an outer sphere and outside an inner sphere centered about a RSO. Such a constraint can be written at time k as

$$s_{min}^2 \leq [\mathbf{x}_{i,k}^{rso} - \mathbf{x}_k]^T \begin{bmatrix} \mathbf{I} & \mathbf{0} \\ \mathbf{0} & \mathbf{0} \end{bmatrix} [\mathbf{x}_{i,k}^{rso} - \mathbf{x}_k] \leq s_{max}^2, \quad (6)$$

where s_{min} is the inner radius and s_{max} is the outer radius of the spheres.

C. Repeating Natural Motion

In an effort to minimize fuel, the formulation includes a quadratic final cost to drive the Chaser into a relative repeating natural orbit. Repeating natural motion is equivalent to enforcing the constraint

$$[\mathbf{I} - \Phi_{k,k+N}] \mathbf{x}_k = \mathbf{0}, \quad (7)$$

where N is the number of time-steps in an orbit.

As a special case using CW equations, (7) collapses to

$$\mathbf{a}^T \mathbf{x}_k = [2n \ 0 \ 0 \ 0 \ 1 \ 0] \mathbf{x}_k = 0, \quad (8)$$

which has an equivalent description in reference [6] using Lawden's equations. Constraint (8) is expressed as a quadratic natural motion cost with scalar weight $W_p > 0$

$$\frac{1}{2} \mathbf{x}_k^T [W_p \mathbf{a} \mathbf{a}^T] \mathbf{x}_k = \frac{1}{2} \mathbf{x}_k^T \mathbf{Q} \mathbf{x}_k. \quad (9)$$

Note, \mathbf{Q} has one non-zero eigenvalue and is positive semi-definite for all positive values of W_p .

D. Optimal Control Problem Formulation

To pose the optimization in terms of impulsive $\Delta \mathbf{v}$ maneuvers, the following definition is made

$$\Delta \mathbf{v} = [\dot{r}_0 \ \dot{s}_0 \ \dot{w}_0]^T - [\dot{r}_{init} \ \dot{s}_{init} \ \dot{w}_{init}]^T$$

where the optimization decision variables are defined as

$$\mathbf{x}(t) = [r(t) \ s(t) \ w(t) \ \dot{r}(t) \ \dot{s}(t) \ \dot{w}(t)]^T,$$

which represent the relative Chaser state in an arbitrary reference orbit using R-S-W (radial, along-track and cross-track directions, respectively) coordinates.

The control cost is written as an initial cost of the form

$$\frac{1}{2} \Delta \mathbf{v}^T \tilde{\mathbf{R}} \Delta \mathbf{v},$$

where $\tilde{\mathbf{R}} = W_r \mathbf{I}_{3 \times 3}$ and $W_r > 0$ is a scalar weight. This can be rewritten in terms of the decision variable \mathbf{x}_0 as

$$\frac{1}{2} \mathbf{x}_0^T \mathbf{R} \mathbf{x}_0 - \mathbf{x}_{init}^T \mathbf{R} \mathbf{x}_0$$

where

$$\mathbf{R} = \begin{bmatrix} \mathbf{0} & \mathbf{0} \\ \mathbf{0} & \tilde{\mathbf{R}} \end{bmatrix}.$$

Combining the control cost and natural motion cost in equation (9), the optimal control problem is a quadratic programming problem written as

$$\inf_{\mathbf{x}} J = \frac{1}{2} \mathbf{x}_0^T \mathbf{R} \mathbf{x}_0 - \mathbf{x}_{init}^T \mathbf{R} \mathbf{x}_0 + \frac{1}{2} \mathbf{x}_T^T \mathbf{Q} \mathbf{x}_T \quad (10)$$

along with the constraints

$$\dot{\mathbf{x}}(t) - f(\mathbf{x}(t)) = \mathbf{0} \quad (11)$$

$$[\mathbf{I} \ \mathbf{0}] \mathbf{x}_0 = \begin{bmatrix} r_{init} \\ s_{init} \\ w_{init} \end{bmatrix} \quad (12)$$

$$\tilde{\alpha} \leq \begin{bmatrix} [\mathbf{x}_{i,0}^{rso} - \mathbf{x}_0]^T \tilde{\mathbf{P}}_0 [\mathbf{x}_{i,0}^{rso} - \mathbf{x}_0] \\ [\mathbf{x}_{i,0}^{rso} - \mathbf{x}_0]^T \Phi_{0,1}^T \tilde{\mathbf{P}}_1 \Phi_{0,1} [\mathbf{x}_{i,0}^{rso} - \mathbf{x}_0] \\ \vdots \\ [\mathbf{x}_{i,0}^{rso} - \mathbf{x}_0]^T \Phi_{0,f}^T \tilde{\mathbf{P}}_f \Phi_{0,f} [\mathbf{x}_{i,0}^{rso} - \mathbf{x}_0] \end{bmatrix} \leq \infty \quad (13)$$

$$s_{min}^2 \leq [\mathbf{x}_{i,T}^{rso} - \mathbf{x}_T]^T \begin{bmatrix} \mathbf{I} & \mathbf{0} \\ \mathbf{0} & \mathbf{0} \end{bmatrix} [\mathbf{x}_{i,T}^{rso} - \mathbf{x}_T] \leq s_{max}^2. \quad (14)$$

The homogeneous dynamic equations are enforced using (11) for $0 \leq t \leq T$. Constraint (12) is a linear constraint on the initial state, and constraints (13) and (14) are non-convex quadratic constraints on the initial and final state, respectively. Because the cost function (10) is quadratic, the formulation is considered a non-convex Quadratic Programming Quadratic Constraint (QPQC) optimization problem. Further, constraints (13) and (14) must be introduced for each RSO with which the Chaser must maintain passive safety.

1) *Receding Horizon Control Stability*: To show that the unconstrained objective function (10) stabilizes the system in an RHC scenario, the following definitions are made:

$$\mathbf{x}_{T_p} = \Phi_{0,T_p} \mathbf{x}_{init} + \begin{bmatrix} \Phi_{0,T_p}^{rv} \\ \Phi_{0,T_p}^{vv} \end{bmatrix} \Delta \mathbf{v}$$

where

$$\Phi_{0,T_p} = \begin{bmatrix} \Phi_{0,T_p}^{rr} & \Phi_{0,T_p}^{rv} \\ \Phi_{0,T_p}^{vr} & \Phi_{0,T_p}^{vv} \end{bmatrix}$$

and T_p is the time between trajectory replanning. Defining

$$\mathbf{B} = \begin{bmatrix} \Phi_{0,T_p}^{rv} \\ \Phi_{0,T_p}^{vv} \end{bmatrix}$$

and substituting into (10), we can define the cost function solely as a function of \mathbf{x}_{init} and $\Delta \mathbf{v}$.

$$J = \frac{1}{2} \Delta \mathbf{v}^T [\tilde{\mathbf{R}} + \mathbf{B}^T \mathbf{Q} \mathbf{B}] \Delta \mathbf{v} + \mathbf{x}_{init}^T \Phi_{0,T_p}^T \mathbf{Q} \mathbf{B} \Delta \mathbf{v} + \frac{1}{2} \mathbf{x}_{init}^T \mathbf{Q} \mathbf{x}_{init}$$

Solving for the minimum of J with respect to $\Delta \mathbf{v}$ produces the optimal impulsive $\Delta \mathbf{v}^*$. For any initial state \mathbf{x}_{init} , the optimal $\Delta \mathbf{v}^*$ is

$$\Delta \mathbf{v}^* = \begin{bmatrix} 0 & 0 & 0 & 0 & 0 & 0 \\ -\frac{2W_p n}{2W_p + W_r} & 0 & 0 & 0 & -\frac{W_p}{2W_p + W_r} & 0 \\ 0 & 0 & 0 & 0 & 0 & 0 \end{bmatrix} \mathbf{x}_{init},$$

or

$$\Delta \mathbf{v}^* = \mathbf{K} \mathbf{x}_{init}.$$

Substituting the minimizing $\Delta \mathbf{v}^*$ back into the impulsive state transition dynamics,

$$\mathbf{x}(T_p) = \Phi_{0,T_p} \mathbf{x}_{init} + \mathbf{B} \Delta \mathbf{v}^* = [\Phi_{0,T_p} + \mathbf{B} \mathbf{K}] \mathbf{x}_{init},$$

it is clear that for any re-plan time T_p (re-plan rate of $\frac{1}{T_p}$), the closed loop RHC dynamics are described by the eigenvalues of $[\Phi_{0,T_p} + \mathbf{B} \mathbf{K}]$ [13]. Because a repeating natural motion is a periodic solution, traditional Lyapunov stability about an equilibrium point cannot be shown. Instead, an approach is taken to show that the repeating natural motion cost drives the system towards stability within a closed invariant set. The approach outlined in [14] is paraphrased, then used to show periodic stability using the repeating natural motion cost. Given a differential system

$$\dot{\mathbf{x}} = f(\mathbf{x}) \quad (15)$$

where $f : D \mapsto R^n$ is a continuously differentiable map from a domain $D \subset R^n$ into R^n . Let $M \subset D$ be a closed invariant set of (15). Define an ε -neighborhood of M by

$$U_\varepsilon = \{\mathbf{x} \in R^n | \text{dist}(\mathbf{x}, M) < \varepsilon\}$$

Where $\text{dist}(\mathbf{x}, M)$ is the minimum distance from \mathbf{x} to a point M ; that is,

$$\text{dist}(\mathbf{x}, M) = \inf_{\mathbf{y} \in M} \|\mathbf{x} - \mathbf{y}\|.$$

Then, the closed invariant set M of (15) is stable if, for each $\varepsilon > 0$, there is $\delta > 0$ such that

$$\mathbf{x}(0) \in U_\delta \Rightarrow \mathbf{x}(t) \in U_\varepsilon, \forall t \geq 0, \quad (16)$$

and asymptotically stable if it is stable and δ can be chosen such that

$$\mathbf{x}(0) \in U_\delta \Rightarrow \lim_{t \rightarrow \infty} \text{dist}(\mathbf{x}(t), M) = 0. \quad (17)$$

To show that the repeating natural motion cost is stabilizing, the closed invariant subset is defined as

$$M_{rnm} = \{\mathbf{x} \in R^n | \mathbf{a}^T \mathbf{x} = 0\}, \quad (18)$$

where \mathbf{a} is defined in equation (8). Therefore, the invariant subset includes all states \mathbf{x} that have repeating natural motions. To illustrate that M_{rnm} satisfies (17), we want to show

$$-\delta < \mathbf{a}^T \mathbf{x}_{init} < \delta \Rightarrow \lim_{t \rightarrow \infty} \mathbf{a}^T \mathbf{x}(t) = 0$$

First, choosing the initial state

$$\mathbf{x}_{init} = [r_{init} \quad s_{init} \quad w_{init} \quad \dot{r}_{init} \quad \dot{s}_{init} \quad \dot{w}_{init}]$$

we see that

$$\mathbf{a}^T \mathbf{x}_{init} = 2nr_{init} + \dot{s}_{init}. \quad (19)$$

Recall that using the minimizing impulsive control $\Delta \mathbf{v}^*$ gives the discrete-time system

$$\mathbf{x}_{T_p} = [\Phi_{0,T_p} + \mathbf{B} \mathbf{K}] \mathbf{x}_{init}$$

and that $t = kT_p$ for any time period $T_p > 0$ and $k = \{1, 2, \dots\}$. Using this relation for $\mathbf{x}(t = T_p)$, $\mathbf{a}^T \mathbf{x}_{T_p}$ simplifies to

$$\mathbf{a}^T \mathbf{x}_{T_p} = \frac{W_r + W_p}{W_r + 2W_p} (2nr_{init} + \dot{s}_{init}). \quad (20)$$

On inspection it is clear that for any $\delta > 0$ bounding (19), $\mathbf{a}^T \mathbf{x}(t = kT_p) \rightarrow 0$ as $t \rightarrow \infty$. The formulation shown in (20) illustrates the closed-loop system is globally asymptotically stable about the invariant set M_{rnm} . Several observations can be made about the closed-loop stability about M_{rnm} . First, given any initial state \mathbf{x}_{init} , the closed loop system will be drawn to the nearest repeating natural orbit defined by $\text{dist}(\mathbf{x}, M_{rnm})$. Second, in the unconstrained case the optimal impulsive maneuvers are always in the s direction, and are only a function of W_r and W_p , and current radial position and along-track velocity (r and \dot{s} , respectively) estimates. Lastly, navigation uncertainty causes the repeating natural motion orbit size to be unbounded; no specific natural motion ellipse size, position on the along-track axis, or W oscillation amplitude is enforced.

2) *Additional Proximity Cost Terms*: In order to mitigate this unbounded behavior, proximity cost terms may be added. The first term

$$W_\varepsilon (4r_T^2 + (s_T^2 - S_c^2) - R_s^2)^2 \quad (21)$$

is minimized on a 2-1 ellipse in the R - S plane with a semi-major axis R_s and location S_c on the along-track axis. Also note, the first cost term does not specify a particular W value, nor any phasing with W oscillation. To keep the W -motion amplitude from becoming unbounded, the following term is added:

$$W_w \left(\frac{w}{R_w} \right)^4 \quad (22)$$

A quartic cost for W -motion is chosen because it is has desirable values for W motion below R_w , then becomes excessively expensive for W motion above R_w . As both (21) and (22) are quartic terms, when they are included as additional terms in (10) the optimization problem becomes a Quartic Program with Quadratic Constraints. While a proof for the stability of RHC with (21) and (22) added to the cost function (10) is not included in this paper, results from example 3 illustrate their effectiveness.

E. Optimizer Choice

The QPQC (both quadratic and quartic) Nonlinear Programming (NLP) problems are formulated using a variant of Collocation developed in [15] and solved using SNOPT. The Collocation formulation uses 4 polynomials of 5th-degree for each decision variable.

III. RESULTS

A simulation is implemented to evaluate the performance of the proposed RHC design. The previously discussed cost (10) and constraints (11, 12, 13, 14) integrated in the OTG software are combined with an orbit propagator into a RHC architecture using MATLAB/SIMULINKTM. The OTG software is compiled C-code wrapped in a SIMULINKTM S-function.

The orbit propagator is modeled as two-body Keplerian motion, and does not contain J2, atmospheric drag, 3rd body effects, and additional higher order environmental disturbances. Uncorrelated white process noise of $2 \times 10^{-5} \frac{m}{s^2}$ is added to the system to represent modeling errors and additional disturbances. A minimum thrust of $0.15 \frac{mm}{s}$ and a maximum thrust limit of $15 \frac{mm}{s}$ are enforced in the simulation (these figures assume a 300kg satellite with 1-lb_f thrusters and a minimum on-time of 10ms). The simulation base time-step is 3s.

The reference orbit is chosen to yield a 90 minute period. The orbit has a semi-major axis of 6652km, an eccentricity of 0, an inclination of 35 deg, an ascending node of 0 deg, an argument of perigee of 0 deg, and an initial true anomaly of 0 deg.

The initial uncertainty covariance matrix $\mathbf{P}(0)$ is defined in each test case by the relative navigation uncertainty. For all test cases, 11 PS constraints ($f = 11$) are added with a total duration of 1 orbit (i.e. the PS constraints guarantee collision avoidance for one orbit). The uncertainty ellipse scaling factor α_k is chosen to be constant for each ellipse with a value of 8. The relative proximity quadratic shell constraint has a lower bound of 10m and an upper bound of 1000m. An upper and lower $\Delta \mathbf{v}$ constraint is enforced with limits of $\pm 100 \frac{mm}{s}$ for each axis. Both W_r and W_p are set to 10^4 (a higher weighting eased numerical scaling difficulties). The RHC horizon time T_h is 900s and the re-plan time T_p is 150s. Because the reference orbit is circular, Hills equations are enforced as trajectory constraints.

Quantitative metrics of interest include total $\Delta \mathbf{v}$, steady-state $\Delta \mathbf{v}/\text{orbit}$, and probability of collision P_{col} . P_{col} is calculated using (5) with the volume \mathbf{V} defined as a 10m cube centered about the Chaser.

A. Example 1: RHC with Repeating Natural Motion and Passive Safety

The first example compares the resulting trajectory, fuel use, stability, and collision probability from an RHC simulation with and without PS constraints. The Chaser and RSO are initialized 100m apart in the along-track axis. Relative navigation uncertainty based on using a carrier-phase GPS sensor is modeled in the RHC simulation as uncorrelated white noise of 0.02m and $0.002 \frac{m}{s}$ for position and velocity, respectively [4,16].

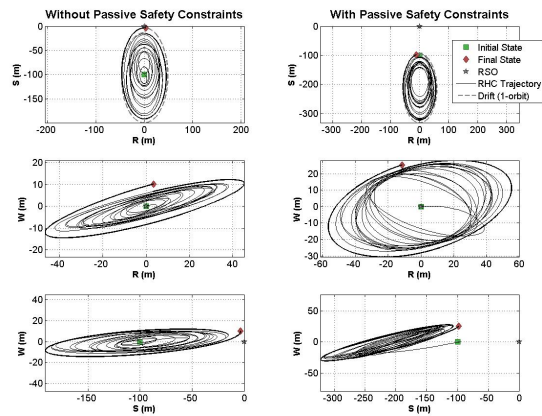


Fig. 2. Example 1: Relative position in R-S, R-W, and S-W Planes

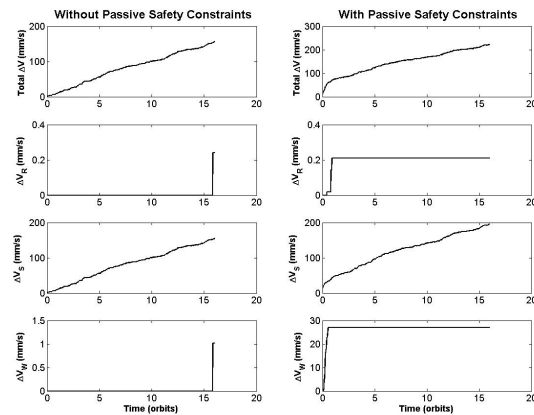


Fig. 3. Example 1: R, S, W, and Total $\Delta \mathbf{v}$ usage

TABLE I
EXAMPLE 1: FUEL USAGE AND COLLISION PROBABILITY COMPARISON

Testcase	Total $\Delta \mathbf{v}$ ($\frac{mm}{s}$)	SS $\Delta \mathbf{v}$ ($\frac{mm}{s}/\text{orbit}$)	Maximum P_{col}
Without PS Constraints	156	9.8	$7.5e^{-2}$
With PS Constraints	223	10.1	$1.6e^{-8}$

Figure 2 depicts the motion of the RSO with respect to the Chaser represented in the rotating R-S-W reference frame fixed to the Chaser. When the PS constraints are included, the Chaser immediately maneuvers away from the along-track

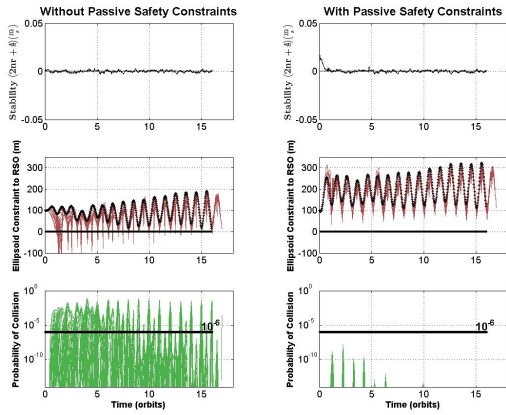


Fig. 4. Example 1: Repeating Natural Motion stability, distance to ellipsoid constraints, and Collision Probability as a function of time

axis with significant out of plane (W) motion. Without PS the Chaser simply attempts to reject process noise disturbance and maintain a repeating natural motion.

Figure 3 compares Δv usage, and illustrates the obvious increase when PS constraints are included, especially in the W axis. The Δv usage due to PS is a function of initial state, relative navigation uncertainty, perturbations, process noise, and desired degree of safety. Examining the total Δv values shown in Table I and Figure 3, the increase in Δv to guarantee PS to the specified collision probability is approximately $67 \frac{m}{s}$. A significant portion of the total increase is attributed to the initial W Δv cost of $28 \frac{m}{s}$ over the first half-orbit. Furthermore, the total SS Δv usage rates, which are calculated from the beginning of orbit 2 to orbit 16, are nearly identical (9.8 vs. $10.1 \frac{m}{s}$ /orbit). The SS Δv usage rates agree after the PS constraints cease to influence the trajectory because both RHC implementations (with and without PS constraints) are equally affected by relative navigation uncertainty and process noise. As suggested in the stability proof II-D.1, Figure 3 confirms optimal maneuvers without influence from PS constraints will involve Δv requests primarily in the S direction. The small Δv usage in R and W observed towards the end of the simulation are attributed to the Chaser approaching the lower bound $10m$ shell constraint.

PS constraint satisfaction (and hypothetical satisfaction for the RHC without such constraints) is displayed in Figure 4 as RSO distance to the PS ellipsoid constraints. Solid dots represent the instantaneous distance between the Chaser and RSO, while thin lines represent distances between PS constraint ellipsoids and the RSO propagated forward for 1 orbit, assuming a failure at that instant. If the RSO distance to the ellipsoids is negative, then the RSO is contained within the ellipsoid. Conversely, instantaneous and propagated distances greater than 0 indicate PS constraint satisfaction.

Similarly, P_{col} is calculated at each replan time, T_p . The current state is propagated forward in time as a drift trajectory (assuming a failure were to occur at that instant) for 1 orbit, along with associated instantaneous P_{col} values.

Table I shows the maximum probability of collision over the 16 orbits, and Figure 4 shows the instantaneous and propagated P_{col} as a function of time. The addition of the PS constraints significantly decreases the probability of collision. Without the PS constraints there is a $7.5e^{-2}$ chance of collision, whereas with PS constraints maximum probability of collision reduces to $1.6e^{-8}$.

The distance of the system from the invariant manifold M_{rnm} (defined in (18) as $2nr + \dot{s} = 0$) as a function of time is calculated and shown in Figure 4. The plot confirms previous stability predictions, as the system distance from M_{rnm} is stable in the presence of relative navigation uncertainty and perturbations. It is interesting to note that the RHC with PS constraints is initially forced to maneuver away from a repeating natural orbit to satisfy the PS constraints. After this deviation, the stability measure quickly approaches the origin and is stable for the remainder of the simulation. Again, the stability proof neither guarantees a particular position on the along-track axis, nor guarantees a particular repeating natural motion ellipse size. This is evident in Figure 2, which highlights relative navigation and perturbations are slowly causing the ellipse to change in size and drift in the along-track axis.

B. Example 2: Effect of Relative Navigation Uncertainty on RHC with Passive Safety Constraints

Example 2 explores the effect of navigation uncertainty on the passive safety RHC implementation. All assumptions and simulation parameters remain the same as the previous example except the relative navigation uncertainty is varied. The $1 - \sigma$ values used for position and velocity in each case are as follows: no navigation uncertainty, $0.01m$ and $0.001 \frac{m}{s}$, $0.02m$ and $0.002 \frac{m}{s}$, $0.03m$ and $0.003 \frac{m}{s}$, $0.04m$ and $0.004 \frac{m}{s}$, and $0.05m$ and $0.005 \frac{m}{s}$.

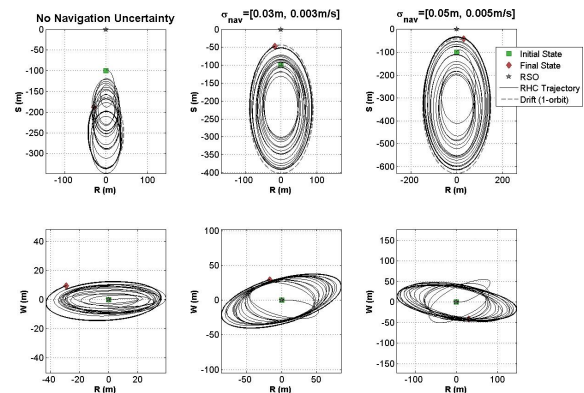


Fig. 5. Example 2: Relative position in R-S, R-W, and S-W Planes

As depicted in Figure 5, increasing relative navigation uncertainty directly affects the PS constraint ellipsoid sizes, which yield increasingly larger repeating natural orbits. Also, cross-axis motion tends to grow as the Chaser avoids intersecting the PS constraint ellipsoid. Ellipse semi-major axis (R_{max}) and cross-axis motion (W_{max}) as a function of navigation uncertainty are summarized in Table II. Passively safe

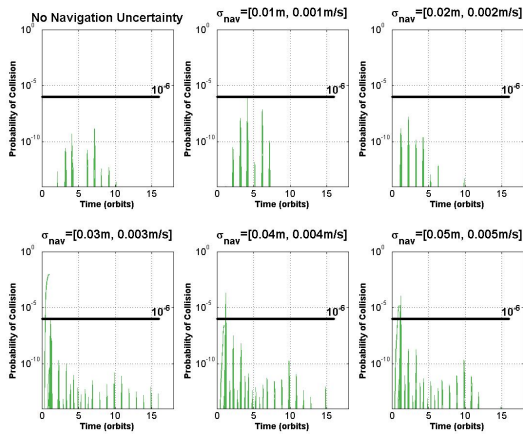


Fig. 6. Example 2: Collision Probability as a function of time

TABLE II

EXAMPLE 2: FUEL USAGE, COLLISION PROBABILITY COMPARISON, AND MOTION IN **R** AND **W**

Testcase	Δv_{tot} ($\frac{mm}{s}$)	SS Δv ($\frac{mm}{s}/orb.$)	Max. P_{col}	R_{max} (m)	W_{max} (m)
No Unc.	35.5	1.0	$1.4e^{-9}$	39.2	12.3
1cm, $1\frac{mm}{s}$	61.1	1.5	$9.4e^{-7}$	46.8	14.1
2cm, $2\frac{mm}{s}$	223	8.5	$1.6e^{-8}$	55.2	28.1
3cm, $3\frac{mm}{s}$	509	22.6	$9.7e^{-3}$	85.9	37.6
4cm, $4\frac{mm}{s}$	933	39.1	$2.0e^{-4}$	111	44.4
5cm, $5\frac{mm}{s}$	1301	58.6	$1.1e^{-4}$	147	55.4

orbits are feasible in the presence of additional navigation uncertainty, but require more fuel.

Table II captures the total Δv and SS Δv for these test cases. As relative navigation uncertainty increases Δv usage also increases. The SS Δv usage rates are calculated using data between orbit 6 and 16. After navigation uncertainty reaches $0.02m$ and $0.002\frac{m}{s}$, Δv usage seems to increase in a linear fashion. For cases with little or no navigation uncertainty, process noise appears to drive Δv usage.

Figure 6 shows the probability of collision to be acceptable for the first three cases, however the last three exhibit values greater than 10^{-6} . In simulation, each of the last three test cases request Δv exceeding the allowed maximum ($\Delta v_{max} = 15\frac{mm}{s}$) on the first time step. In this situation, Δv_{max} is used instead. Since the initial Δv is not executed as requested, the PS constraints are not satisfied. The RHC continues to request Δv exceeding Δv_{max} for the first few replan steps until the PS constraints are satisfied without exceeding maximum Δv limitations. To summarize, limiting requested Δv results in larger initial collision probabilities, however after Δv requests decrease again, the PS constraints ensure acceptable levels of collision probability.

Given a fixed tolerance for collision probability, increased navigation uncertainty increases relative natural motion distance from the RSO. This relationship directly links mission-level collision probability requirements and desired relative maneuver range with relative navigation uncertainty requirements.

C. Example 3: RHC with and without Proximity Cost

The relative orbits resulting in Examples 1 and 2 illustrate the unbounded behavior in ellipse size, location on the along-track axis, and W oscillation amplitude as discussed in section II-D.1. Although such behavior does not violate the PS constraints, certain proximity operation missions may desire more stringent control over the resulting relative orbit geometry. This can be achieved by implementing the proximity cost terms from equations (21) and (22) discussed in section II-D.2. Example 3 compares simulation results when the proximity cost terms are included with the PS results from Example 1. The values chosen for S_c , R_s , R_w , W_e and W_w are $-200m$, $100m$, $100m$, $3e^{-7}$ and 1 , respectively. Results show PS constraints are satisfied even when more stringent control over the relative orbit geometry is desired.

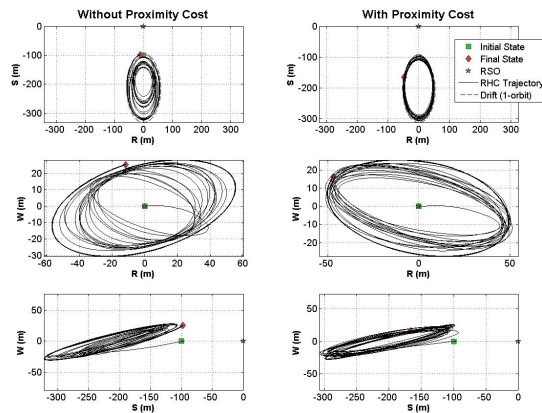


Fig. 7. Example 3: Relative position in R-S, R-W, and S-W Planes

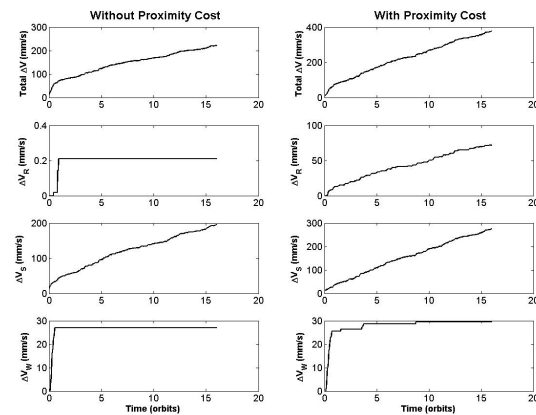


Fig. 8. Example 3: R, S, W, and Total Δv usage

For convenient comparison, the passive safety results from Example 1 are repeated in Figures and Tables for this example. Results in Figure 7 show the Chaser, initially $100m$ behind the RSO, maneuver to the specified relative orbit centered $200m$ behind the RSO that projects a 100×200

TABLE III

EXAMPLE 3: FUEL USAGE AND COLLISION PROBABILITY COMPARISON

Testcase	Total Δv ($\frac{mm}{s}$)	SS Δv ($\frac{mm}{s}/orbit$)	Maximum P_{col}
Without Proximity Cost	223	10.1	$1.6e^{-8}$
With Proximity Cost	377	20.3	$1.2e^{-7}$

meter ellipse in the R - S plane. Also, the varying ellipse size and S location is eliminated at the expense of more fuel.

Figure 8 shows the increased Δv introduced by the proximity cost terms. Comparing with the passive safety values repeated in Table III, Δv usage is up $104 \frac{mm}{s}$ totaling $377 \frac{mm}{s}$ for 16 orbits. Furthermore, the SS Δv usage rate defined in Example 1 doubles to $20.3 \frac{mm}{s}/orbit$. The additional usage is attributed to the frequent burns in R and S to maintain the desired relative orbit in the presence of navigation uncertainty and process noise. Also, W_w is selected sufficiently small to not penalize the W position until the Chaser approaches the R_w value of $100m$. The R_w threshold is never approached in the simulated example and causes little Δv impact. Thus, the PS constraints remain the primary driver for burns in the W direction.

Even though additional Δv is required when the proximity cost terms are included, the stability and passive safety metrics are virtually unaffected. Maximum probability of collision shown in Table III at $1.2e^{-7}$ remains well below the design threshold of 10^{-6} .

IV. CONCLUSIONS

Recent on-orbit mission performance illustrates a pressing need to develop relative navigation trajectories and controllers that minimize collision probability. Current passive safety approaches do not stochastically account for relative navigation uncertainty and its intimate connection with collision probability, deal with satellite failures between optimizer time steps, quickly react to changing relative states or active RSOs, or address admissible classes of repeating relative natural motion trajectories. Constraints are developed for general Linear, Time-Varying (LTV) systems to explicitly account for in-situ relative navigation performance and guarantee desired passive safety metrics. The passive safety constraints are incorporated into a RHC implementation along with relative state constraints. The stability of the unconstrained RHC is proven for all relative states in which CW equations are valid, and for all replan rates. A Keplerian simulation including gaussian process noise is used to evaluate the performance of the RHC, the effects and costs of the passive safety constraints, and the effects of relative navigation uncertainty. The passive safety constraints developed in this paper are found to greatly decrease collision probability at the expense of modestly increased Δv usage. Examples 1, 2, and 3 suggest that traditional proximity operations trajectories, such as perching on the along-track axis or executing circumnavigations exclusively in the R - S -plane are not passively safe. Relative navigation uncertainty is confirmed to be a significant driver for both Δv usage and feasible relative distance. Additional proximity costs are

found to moderate unbounded behavior in relative motion ellipse size and along-track axis location. Further work may include proving RHC stability for Lawden's equations, proving global multi-satellite distributed system stability in the presence of passive safety constraints, deriving optimal deadband relations for the RHC implementation, and fully exploring passive safety Δv cost as a function of navigation uncertainty, non-linear perturbations, process noise, and acceptable collision probability.

REFERENCES

- [1] *Overview of the DART Mishap Investigation Results*, NASA.gov, http://www.nasa.gov/pdf/148072main.DART_mishap_overview.pdf, last accessed December, 2007.
- [2] L. Breger, J. How, *Safe Trajectories for Autonomous Rendezvous of Spacecraft*, AIAA Guidance, Navigation and Control Conference, Aug 2007. AIAA-2007-6860.
- [3] M. Mitchell, L. Breger, J. P. How, *Effects of Navigation Filter Properties on Formation Flying Control*, AIAA Guidance, Navigation, and Control Conference and Exhibit, August 2004. AIAA 2004-5024.
- [4] J. P. How, M. Tillerson, *Analysis of the Impact of Sensor Noise on Formation Flying Control*, Proceedings of the American Control Conference, June 2001. 0-7803-6495-3.
- [5] M. E. Campbell, *Collision Monitoring Within Satellite Clusters*, IEEE Transactions of Control Systems Technology, Vol 13, No. 1, 2005.
- [6] M. Tillerson, G. Inalhan, J. P. How, *Co-ordination and Control of Distributed Spacecraft Systems using Convex Optimization Techniques*, International Journal of Robust and Nonlinear Control, 2002, 12:207-242.
- [7] L. S. Breger, G. Inalhan, M. Tillerson, J. P. How, *Cooperative Spacecraft Formation Flying: Model Predictive Control With Open-And Closed-Loop Robustness*, Modern Astrodynamics, Elsevier, Oxford, 2006.
- [8] D. F. Lawden, *Optimal Trajectories for Space Navigation*, Butterworths, London, 1963, pp. 79-86.
- [9] G. Hill, *Researches in the Lunar Theory*, American Journal of Mathematics, Vol 1, 1878, pp. 5-26.
- [10] W. H. Clohessy, R. S. Wiltshire, *Terminal Guidance System for Satellite Rendezvous*, Journal of Aerospace Sciences, Vol 27, No. 9, 1960, pp. 653-658.
- [11] A. Gelb, J. F. Kasper, R. A. Nash, C. F. Price, A. A. Sutherland, *Applied Optimal Estimation*, The M.I.T. Press, Cambridge, Massachusetts, 1974.
- [12] A. J. Chorin, O. H. Hald, *Stochastic Tools in Mathematics and Science*, Springer Science & Business Media, Inc., 2006.
- [13] G. F. Franklin, J. D. Powell, M. Workman, *Digital Control of Dynamic Systems*, 3rd Ed., Addison Wesley Longman Inc., Menlo Park, California, 1998.
- [14] H. K. Khalil, *Nonlinear Systems*, 3rd Edition, Pearson Education, Upper Saddle River, 2000.
- [15] M. B. Milam, *Real-time optimal trajectory generation for constrained dynamical systems*, PhD Dissertation, California Institute of Technology, 2003.
- [16] F. D. Busse, J. P. How, *Real-time Experimental Demonstration of Precise Decentralized Relative Navigation for Formation Flying Spacecraft*, AIAA Guidance, Navigation, and Control Conference and Exhibit, August 2002. AIAA-2002-5003.